

FedRel: An Adaptive Federated Relevance Framework for Spatial Temporal Graph Learning

Tiehua Zhang*, Member, IEEE, Yuze Liu*, Zhishu Shen, Member, IEEE, Rui Xu, Xin Chen, Xiaowei Huang, Xi Zheng, Member, IEEE,

Abstract—Spatial-temporal data contains rich information and has been widely studied in recent years due to the rapid development of relevant applications in many fields. For instance, medical institutions often use electrodes attached to different parts of a patient to analyse the electorencephal data rich with spatial and temporal features for health assessment and disease diagnosis. Existing research has mainly used deep learning techniques such as convolutional neural network (CNN) or recurrent neural network (RNN) to extract hidden spatial-temporal features. Yet, it is challenging to incorporate both inter-dependencies spatial information and dynamic temporal changes simultaneously. In reality, for a model that leverages these spatial-temporal features to fulfil complex prediction tasks, it often requires a colossal amount of training data in order to obtain satisfactory model performance. Considering the above-mentioned challenges, we propose an adaptive federated relevance framework, namely FedRel, for spatial-temporal graph learning in this paper. After transforming the raw spatial-temporal data into high quality features, the core Dynamic Intra-Intra Graph (DIIG) module in the framework is able to use these features to generate the spatial-temporal graphs capable of capturing the hidden topological and long-term temporal correlation information in these graphs. To improve the model generalization ability and performance while preserving the local data privacy, we also design a relevance-driven federated learning module in our framework to leverage diverse data distributions from different participants with attentive aggregations of their models. In addition, we conduct extensive experiments on two real-world spatial-temporal datasets. The results demonstrate the effectiveness of our proposed framework in spatial-temporal interpretation, collaborative model training, and divergent data distribution handling in most settings of comparison.

Index Terms—Spatial-temporal Data, Collaborative Graph Learning, Distribution-based Relevance, Graph Neural Network.

I. INTRODUCTION

IN recent years, spatial-temporal data has drawn increasing attention owing to its great potential in various fields and significant effects on daily activities such as traffic management [1], health monitoring [2], and action recognition [3]. The advancement of deep learning has shed light on processing

Tiehua Zhang, Yuze Liu, Rui Xu, Xin Chen and Xiaowei Huang are with Ant Group, Shanghai, China (e-mail: {zhangtiehua.zth, liuyuze.liuyuze, furui.xr, jimming.cx, wei.huangxw}@antgroup.com).

Zhishu Shen is with the School of Computer Science and Artificial Intelligence, Wuhan University of Technology, Wuhan, China (e-mail: z_shen@ieee.org).

Xi Zheng is with the Department of Computing, Macquarie University, Sydney, Australia (e-mail: james.zheng@mq.edu.au).

* co-first authorship. (Corresponding author: Tiehua Zhang)

Copyright (c) 20xx IEEE. Personal use of this material is permitted. However, permission to use this material for any other purposes must be obtained from the IEEE by sending a request to pubs-permissions@ieee.org.

by extracting valuable features from spatial-temporal data to facilitate the downstream prediction/regression tasks. For instance, traditional deep learning techniques such as convolutional neural networks (CNNs) [2] and recurrent neural networks (RNNs) [4], [5] have been heavily investigated to uncover the hidden correlations and interdependencies in spatial-temporal data sequence.

Even though the existing models are able to capture and utilise the extracted correlation to some extent, many limitations start surfacing: CNN-based methods face challenges in discovering long-term temporal correlations while RNN-based ones lack the capability to comprehend the global spatial structure. Additionally, one common issue is that both model types require the grid-like data input, which is considered intractable when decoding the topological information from the spatial dimension. It is argued that the non-Euclidean graph data structure shows great potential in terms of representing inter-connectivity and dynamic trends in both spatial and temporal aspects [6]. Recently, modelling the spatial-temporal data into graph representation has risen to the spotlight owing to the development of graph neural network (GNN), reporting some encouraging improvements on both classification and regression tasks compared with CNN and RNN based models [7], [8]. It is also proven in prior work [9] that even for data in which explicit graph structure does not naturally exist, extracting and modelling the hidden graph structure from the original data could lead to a significant performance improvement. Following that, most existing methods [7], [8], [10], [11] first transform spatial-temporal data into the static graphs by modelling both nodes and edges, and then use GNNs to learn the embedding representations from the generated static graphs. Taking the traffic flow graph as an example in which different districts are treated as nodes, the flow of traffic between nodes will experience the changes at different hours of the day [1]. Ignoring dynamic correlations between nodes in the temporal dimension will undoubtedly lead to compromised and less desirable results. It is thus crucial to capture the inter-dependencies and dynamic temporal changes over time when turning the spatial-temporal data into the graph structure.

Apart from the quest to utilise spatial-temporal data more effectively, another pressing problem regards the data scarcity issue in real-world applications. For all learning-based tasks, insufficient data essentially causes an over-fitting problem of the model and make it hard to generalise when unseen data appears during inference time. One common way to solve this problem is to collect a colossal amount of training data from multiple parties and train the model in a centralised manner.

However, it has drawn increasing concerns over data privacy and security in many data-sensitive institutions. For instance, hospitals and drug research institutions rarely publish patient and clinical data due to their sensitivity, and trainable models thus fail to infer results that are not present in the training set. To this end, federated learning (FL) [12] is introduced as a collaborative training scheme, which involves multiple parties without exposing local data to others. By integrating all participants' model weights or gradients, the model trained by FL will thus have a higher generalisation ability.

In the commonly used FL framework [13], all participants' data is by default in the same distribution, while in real-world cases, the divergence of data distribution from different participants is nontrivial since it is determined by many uncontrollable factors like separate geographic locations. The most prevalent FL algorithm is called FedAvg [13], in which the local model weights are sent to the server and aggregated in an iterative manner. However, it ignores the non-IID data distribution fact and assumes equal contribution from all participants. It is thus both intuitive and critical to incorporate the difference in data distribution from participants and make it part of FL process to facilitate the training process.

In this work, we propose a novel adaptive federated relevance framework called FedRel for spatial-temporal graph learning. This framework is composed of three key modules, including a feature transformation net to extract the important spatial-temporal features from raw data, a dynamic inter-intra graph (DIIG) module to generate the spatial-temporal graphs while capturing inter-dependencies and dynamic temporal changes across these graphs, and a relevance-based federated learning module to expedite the collaborative graph learning. It is worth mentioning that the intra-graph concept in our work refers to the spatial node correlations inside one generated spatial graph at any timestamp, while inter-graphs indicate temporal node correlations across multiple spatial graphs. The main advantages of our proposed framework are two folds: 1) DIIG uncovers the hidden topological graph structures of the transformed spatial-temporal features, which effectively encodes both spatial and temporal information into the embedding space when updating the node embedding through the GNN model; 2) The DIIGs from different participants are an integral part of the federated relevance training process. Thus the models are trained collaboratively to enable a better generalisation capability.

The contributions of this work are summarised as follows:

1. We propose a novel adaptive federated relevance framework, namely FedRel, for spatial-temporal graph learning. The relevance of each participant is determined by adaptively attending the distance scores between local data distribution and the approximated global distributions, enabling the framework to put more attention on the participants with divergent data distributions and improve model's generalisation ability.
2. We implement several variants of feature transformation nets using a variety of model structures with different design philosophies, aiming to find the most practical model that excels in processing spatial-temporal raw

data and is capable of generating high-quality spatial-temporal features.

3. We conceptualise the inter-intra graphs learning from spatial-temporal features. We also design and implement a dynamic inter-intra graph (DIIG) module to generate the spatial-temporal graphs so as to capture inter-dependencies and dynamic temporal changes across these graphs.
4. We conducted a comprehensive experiment of our framework on real-world dataset ISRUC_S3 [14] and SHL_Small [15], along with detailed ablation studies on each module for the interpretability purpose. The experimental results show that the proposed model achieves promising results in task-specific classifications, model convergence performance, and scalability.

II. RELATED WORK

A. Deep Learning for Spatial-Temporal Data

The study of spatial-temporal data has attracted increasing attention in recent years, especially after the emergence of many advanced deep learning models. It is pointed out that spatial-temporal data could benefit applications in many disciplines such as emotion detection, traffic flow prediction, and sleep stage/quality classification [6]. However, It has been a long-standing challenge to better uncover and understand the hidden attributes in these numeric data.

Recent research tries to interpret spatial and temporal dependencies, of which the deep learning model could take advantage to generate better prediction/classification results. For instance, a fast discriminative complex-valued convolutional neural network (CNN) [2], namely FDCCNN, is designed to apprehend the hidden correlations in the electroencephalogram (EEG) signals to expedite the sleep stage classification task. Alternatively, MLP-Mixer [16] is also used in the multi-channel temporal signal data, resulting in promising results on the regression task. It is proven effective to use recurrent neural network (RNN) based models for capturing non-linear interdependencies, including ConvLSTM [4], Bi-LSTM [5]. Following that, some studies start to use the attention mechanisms for capturing the long-term correlations [17]. Specifically, relevant spatial and temporal attention modules are designed to serve this purpose, reporting promising results in clustering multivariate time series data with varying lengths.

B. Graph Neural Networks (GNNs)

Although applying CNN and RNN to spatial-temporal data has yielded promising results, the limitations are also clear. First, both of these techniques still require processing data in the Euclidean space, essentially ignoring the potential connectivity information in the spatial dimension. Also, the inter-dependent relations uncovered using both methods are difficult to interpret from human's perspective. The rise of GNN has shed light on this direction as some researchers have started investigating how to use graphs to form better topological representations in both spatial and temporal dimension [18].

However, constructing graph structure from the spatial-temporal data is the prerequisite before using GNN models,

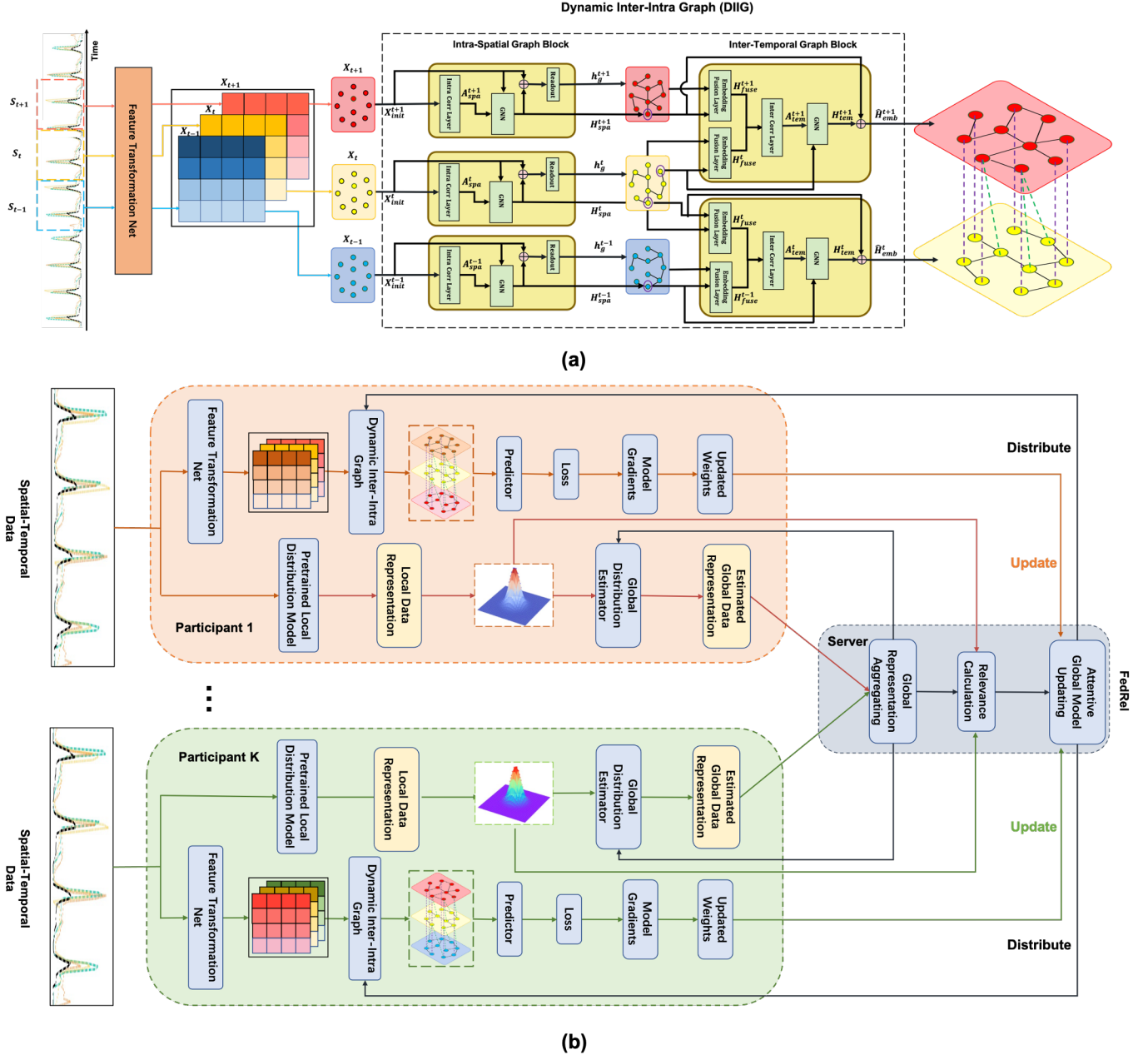


Fig. 1. The overview of the FedRel (better viewed in color): (a) an example of exacting spatial-temporal features from the raw input data. In dynamic inter-intra graph (DIIG) module, The intra-spatial graph block first takes the initial node features at each timestamp to update embedding for each spatial graph. The inter-temporal graph block then merge across different spatial graphs in temporal dimension, producing the embedding with both spatial and temporal information; (b) the process of collaborative training on DIIGs from different participants. It enables an attentive model aggregation based on the relevance-guided divergence between local data distributions and approximated global data distribution.

and there are two main hurdles when transforming the spatial-temporal sequence to GNN-required graph input: 1. to uncover the spatial correlations of the data streams to generate the adjacency matrix; 2. to extract the node features from the temporal values. A line of research has focused on solving this issue [7], [8], [10], [11]. Specifically, graph convolutional recurrent network (GCRN) [10] combines the LSTM network with ChebNet [19] to handle spatial-temporal data. Structural-RNN [7] uses node-level and edge-level RNN to uncover spatial correlations in the data. Alternatively, CNN could be used to embed temporal relationships to solve the explod-

ing/vanishing gradient problems. For example, ST-GCN [11] uses the partition graph convolution layer to extract spatial information, while a one-dimension convolution layer is designed to extract temporal dependencies. Similarly, CGCN [8] combines a one-dimension convolution layer with a ChebNet or GCN layer, to handle spatial-temporal data. Regardless of using the CNN-, RNN-based models, or the recent advancements on GNN-based ones, the existing research is not able to utilise the underlying topological graph structures and temporal transition information in the spatial-temporal data simultaneously, and we intend to deal with this issue in our

work.

C. Federated Learning (FL)

Federated Learning is a privacy-preserving collaborative learning paradigm designed to protect participants' local data privacy while enjoying a superior model performance. It enables the communication of participants' local gradients/weights to avoid exposing the raw data to others. FL is considered helpful in many fields, where data privacy is a major concern [20]. One of the widely used FL algorithms is FedAvg [13], in which the local model weights are sent to the server and aggregated in an iterative manner. However, due to the diversity and divergence of local data distribution, the performance of FL is greatly compromised. It is pointed out in [21] that the non-IID data distribution from different participants lead to severe weight divergence throughout the training phase. To cope with that, [21]–[23] propose to generate part of the global dataset by sharing some local data with the server so that the negative impact of non-IID could be mitigated. But the problem is obvious: it violates the design philosophy of FL by exposing partial data to others. Following that, Shin et al. [24] proposes to upload XOR encoded seeds from participants' local data to the server for the global data approximation. The global data is decoded using these seeds to re-train the model at server side. Instead of simply averaging the local model weights that causes the weight divergence, the contributions from different participants should be considered to facilitate the convergence of training. By calculating the distance between global and participant models at every communication round, attention scores are calculated as weighting coefficients on each local model when being aggregated [25]. Instead of considering the weight distance or violating the local data privacy in other works, we believe the divergent local data distribution from different participants could contribute greatly when it comes to producing a well-performing model. In the FL process of our work, we intend to explore how the local data distribution and approximated global distribution could facilitate the training. The relevance of each participant is quantified and incorporated during training to generalise the model well.

III. PRELIMINARIES

A. Spatial-Temporal Graph

A spatial-temporal data can be represented as $\mathcal{S} = \{\mathbf{S}(1), \mathbf{S}(2), \dots, \mathbf{S}(T)\} \in \mathbb{R}^{T \times N \times D}$, where $\mathbf{S}(t) = [s_1(t), s_2(t), \dots, s_N(t)] \in \mathbb{R}^{N \times D}$, $t \in [1, 2, \dots, T]$, is the time series, and $s_n(t) \in \mathbb{R}^D$, $n \in [1, 2, \dots, N]$, represents the original signal feature dimension D at n th channel in temporal context. N indicates the number of channels in the spatial dimension (e.g., devices and sensors). For each $\mathbf{S}(t)$, the features generated by the feature transformation net is $\mathbf{X}(t) = [x_1(t), x_2(t), \dots, x_N(t)] \in \mathbb{R}^{N \times d}$, where d is the size of the extracted features (As shown in the left part of Fig. 1.a).

To model the inter-dependencies over time steps, we define a time window w to capture the historical sequence in temporal context, i.e., $\{\mathbf{X}(t-w), \dots, \mathbf{X}(t)\}, w \in [0, 1, \dots, t-1]$. We

TABLE I
TABLE OF IMPORTANT NOTATIONS

Notation	Description
\oplus	Concatenation operation
$ \cdot $	The set size
$\ \cdot\ _2$	L2 norm
$f_{mn}(\cdot)$	Row-wise mean function
$\mathcal{N}(\cdot)$	Multivariate Gaussian function
$\sigma(\cdot)$	Sigmoid activation function
$\text{softmax}(\cdot)$	Softmax function
$\exp(\cdot)$	Exponential function
$\text{MSE}(\cdot)$	Mean square error function
$\text{LN}(\cdot)$	Layer normalisation
$\text{msg}(\cdot)$	Message passing function
$\text{readout}(\cdot)$	Graph readout function
$g_\theta(\cdot)$	Global distribution estimator
\mathcal{L}	Loss function
w	Window size
N	The number of channels/nodes
K	The number of participants
T	Time steps
D	Raw data signal dimension
d	Feature dimension
L	Largest message passing layers
\mathcal{S}	A set of raw spatial-temporal raw data
\mathbf{S}	Spatial-temporal feature matrix
s_n	A row of raw signal frequency from \mathcal{S}
\mathcal{X}	A set of initial node features
\mathbf{X}	Initial node feature matrix of a graph
\mathbf{x}_i	Initial feature vector of node v_i
\mathcal{G}	A graph
\mathcal{V}	The set of nodes in the graph
\mathcal{E}	The set of edges in the graph
v	A node $v \in \mathcal{V}$
$e_{i,j}$	Edge between v_i and v_j
\mathbf{A}	Adjacency matrix of a graph
$A_{i,j}$	Correlation value between nodes v_i and v_j
$\mathcal{G}_{spa}(t)$	Spatial graph at t th time step
$\mathcal{G}_{tem}(t)$	A stack of spatial graphs within a time window
$\tilde{\mathbf{S}}^{(k)}$	Reshaped local dataset at participants k
$\tilde{\mathbf{s}}_i^{(k)}$	A local data sample from $\tilde{\mathbf{S}}^{(k)}$ at participant k
\mathbf{H}	node embedding matrix at a graph
h_i	node v_i 's embedding vector
$\tilde{\mathbf{z}}$	Predictor output
\mathbf{y}	True label
\mathbf{z}	Latent data representation of one local data point
\mathbf{d}	Latent representation of local data
$\tilde{\mathbf{d}}$	Synthesised global data representation
\mathbf{I}	Identity matrix
$\mathbf{W}, \Theta, \theta, \theta_S$	Learnable model parameters

define a graph as $\mathcal{G} = (\mathcal{V}, \mathcal{E}, \mathbf{A})$, where $\mathcal{V} = \{v_1, \dots, v_N\}$ is the set of nodes, and $\mathcal{E} = \{(v_i, v_j) | v_i, v_j \in \mathcal{V}\}$ denotes the set of edges in the graph, which can be quantified by an adjacency matrix $\mathbf{A} \in \mathbb{R}^{|\mathcal{V}| \times |\mathcal{V}|}$. The $A_{i,j} > 0$ means there exists an edge $e_{i,j}$ between v_i and v_j , and $A_{i,j} = 0$ otherwise.

Since there is no explicit graph structure in the extracted feature $\mathbf{X}(t)$, we use spatial channels to represent nodes in our problem setting, meaning $|\mathcal{V}| = N$, which then is referred as a spatial graph \mathcal{G}_{spa} . The temporal graph, on the other hand, is composed of a stack of spatial graphs in time window w , which is denoted as Given $\mathcal{G}_{tem}(t) = [\mathcal{G}_{spa}(t-w), \mathcal{G}_{spa}(t-w+1), \dots, \mathcal{G}_{spa}(t)]$.

B. Graph Neural Networks (GNNs)

GNN works on the graph structure data and presents an effective way of learning both node and graph embeddings. It requires both initial node features and adjacency matrix as the input, and conducts the layer-based message passing to aggregate neighboring nodes information and update embeddings [26]. Given any $\mathcal{G} = (\mathcal{V}, \mathcal{E}, \mathbf{A})$, the message passing function can be formalised as a function $msg(\cdot)$ with trainable weights:

$$\mathbf{H}^l = msg(\mathbf{A}, \mathbf{H}^{l-1}) \quad (1)$$

$$msg(\mathbf{A}, \mathbf{H}^{l-1}) = \sigma \left(\mathbf{W}_{agg}^l \cdot \left(\mathbf{H}^{l-1} \oplus \frac{1}{N} \cdot \mathbf{A} \cdot \mathbf{H}^{l-1} \right) \right) \quad (2)$$

where $l = 1, \dots, L$ denotes the message passing layer. $\mathbf{h}_i^l \in \mathbf{H}^l$ is updated embedding of node v_i , and \mathbf{W}_{agg}^l is the trainable weight matrix at that layer. Note it exists $\mathbf{H}^0 = \mathbf{X}$ at the initial stage, using the initial node features as the embedding information. \oplus is the vector concatenation operation, and $\sigma(\cdot)$ is the activation function.

To derive the graph representation after the iterative updates of node embeddings, a graph readout function can be defined as $readout(\cdot)$:

$$\mathbf{h}^G = readout(\mathbf{H}^L, \mathbf{X}) \quad (3)$$

$$readout(\mathbf{H}^L, \mathbf{X}) = \sigma \left(\mathbf{W}_{pool} \cdot \left(\frac{1}{N} \sum_{i=1}^N \mathbf{h}_i^L \oplus \mathbf{x}_i \right) \right) \quad (4)$$

where \mathbf{H}^L denotes the up-to-date node embeddings after L th message passing, and \mathbf{h}^G denotes the embedding representation of the graph derived from \mathbf{H}^L . We use a trainable weight \mathbf{W}_{pool} as the linear transformation pooling, which can also be replaced by alternative operations such as min-pooling, max-pooling, or attentive-pooling [27].

C. Federated Learning (FL)

Federated learning is a collaborative training protocol to learn a well-generalised model without exposing the local participants' data to others. It enables the trainable weight aggregation on the server side. FL encompasses several rounds of training, in which each participant uploads the locally trained model to the server for model aggregation (e.g., FedAvg algorithm [13]). The updated model is then distributed back to participants. FL repeats this training protocol until the model converges. The objective function to minimise at the server side is:

$$\min_{\Theta} F(\Theta) : \text{where } F^{(k)}(\Theta) = \sum_{k=1}^K r^{(k)} F(\Theta)^{(k)} \quad (5)$$

where K is the number of participants. $r^{(k)} \geq 0$ is the weighting coefficient of participant k for attentively aggregating the uploaded weights, where $\sum_{k=1}^K r^{(k)} = 1$. $F(\Theta)^{(k)}$ is the local objective function of participant k where Θ is the trainable

weight sets at that participant. Note that in FedAvg the $r^{(k)}$ is set to be $1/K$, meaning this algorithm considers equal contribution of each participant.

IV. DETAILS OF FEDREL

The overview of the architecture of the FedRel is shown in Fig. 1. We elaborate on the proposed framework in this section and formalise the four key components of the framework: 1) transforming the raw spatial-temporal data to high-quality initial node features; 2) intra-spatial graph block to uncover the attentive spatial correlations of different nodes and update node embedding per spatial graph; 3) inter-temporal graph block to incorporate the inter-dependencies into node embedding among neighbouring spatial graphs in temporal dimension; 4) FL relevance module for attentive weight aggregation based on divergent data distribution. The important notations appeared in this paper are summarised in Table I.

A. Feature Transformation Net

Since GNN requires both node features and adjacency matrix, the framework first takes the spatial-temporal sequence data as the raw input, followed by the designated feature transformation net to generate the initial node features matrix $\mathbf{X}(t)$ at each time step t (Fig. 1.a). The feature transformation net can be implemented using variants of prevalent deep learning models, and the commonly used ones are CNN and RNN-based models [4], [5], [28]. It is already clarified in Section III-A that the raw sequence data $\mathcal{S} = \{\mathbf{S}(1), \mathbf{S}(2), \dots, \mathbf{S}(T)\} \in \mathbb{R}^{T \times N \times D}$, the feature transformation process can be defined as:

$$\{\mathbf{X}(1), \dots, \mathbf{X}(t)\} = transform(\{\mathbf{S}(1), \dots, \mathbf{S}(t)\}; \theta_S) \quad (6)$$

where θ_S is the trainable parameters in the feature transformation net, and $\mathcal{X} = \{\mathbf{X}(1), \mathbf{X}(2), \dots, \mathbf{X}(t)\} \in \mathbb{R}^{T \times N \times d}$ is the high-quality output, i.e. the generated initial node features. Note the feature transformation is performed as the local process at each participant, so it serves as the local pre-trained model and differs the θ_S in different participants.

B. Dynamic Inter-Intra Graph (DIIG) Module

The dynamic inter-intra graph encompasses two primary goals: 1) to enable the intra-graph embedding update through the intra-spatial graph block, which uncovers the hidden correlations between spatial nodes and update node embedding in spatial dimension; 2) to further encode temporal changes of these spatial graphs and update the node embedding with these inter-dependencies in the time axis, in which the inter-node correlations between two adjacent spatial graphs are also quantified in the inter-temporal graph block.

1) *Intra-Spatial Graph Block*: The intra-spatial graph block defines a spatial graph at any time t based on the generated initial node features $\mathbf{X}(t) \in \mathbb{R}^{N \times d}$ from the feature transformation net. As explained in Section III-B, we deploy GNN for intra-graph learning, while updating the embedding of each node based on the correlations with spatial neighbour. We have reported using different static correlation functions in

our preliminary work [28], including PCC, PLV, and K -NN. Simply, these static correlation functions take a node feature matrix as the input, and use different ways of quantifying a numeric value based on a pair of node features (details of each explained in Section V-A). However, the shortcomings of using the static functions are obvious: 1) the connectivity between nodes will not change along with dynamic changes of node embedding; 2) it is unable to form the correlations between nodes residing in different graphs. To solve that, we design a dynamic intra correlation layer $c(\cdot, \cdot)$ to generate the correlation of two nodes, which is calculated as:

$$A_{spa}^{i,j}(t) = c(\mathbf{x}_i(t), \mathbf{x}_j(t)) = \frac{\exp\left((\mathbf{x}_i(t))^T \cdot \mathbf{W}_{spa} \cdot \mathbf{x}_j(t)\right)}{\sum_{n=1}^N \exp\left((\mathbf{x}_i(t))^T \cdot \mathbf{W}_{spa} \cdot \mathbf{x}_n(t)\right)} \quad (7)$$

where $\mathbf{x}_i, \mathbf{x}_j \in \mathbb{R}^{1 \times d}$. $\mathbf{W}_{spa} \in \mathbb{R}^{d \times d}$ is a learnable weight matrix and used to project the feature vectors into the correlation space, from which a correlation scalar between node v_i and v_j can be learnt dynamically. The softmax operation serves two purposes: 1) to ensure the non-negative correlation value; 2) to normalise the value between 0 and 1. The iterative calculation of each pair in the feature matrix $\mathbf{X}(t)$ leads to the full adjacency matrix $\mathbf{A}_{spa}(t)$ of this spatial graph $\mathcal{G}_{spa}(t)$.

As mentioned in Section III-B, the embedding update of $\mathcal{G}_{spa}(t)$ using GNN can be formalised as:

$$\mathbf{H}_{spa}^l(t) = msg\left(\mathbf{A}_{spa}(t), \mathbf{H}_{spa}^{l-1}(t)\right) \quad (8)$$

where $l = 1, \dots, L$ denotes the message passing layer, and $\mathbf{H}_{spa}^0(t) = \mathbf{X}(t)$. We have $\mathbf{H}_{spa}^L(t) = [\mathbf{h}_1^{spa}(t), \mathbf{h}_2^{spa}(t), \dots, \mathbf{h}_N^{spa}(t)]$ as the up-to-date node embeddings in $\mathcal{G}_{spa}(t)$, and the graph embedding of which can be calculated as:

$$\mathbf{h}^{\mathcal{G}}(t) = readout\left(\mathbf{H}_{spa}^L(t), \mathbf{X}(t)\right) \quad (9)$$

Eq.8 and Eq.9 essentially provide the embeddings of nodes and graph at each timestamp, which are then taken as the input to Inter-temporal graph block for embeddings update in temporal dimension.

2) *Inter-Temporal Graph Block*: After obtaining the embeddings of nodes and graph at the spatial graph level, it is critical to incorporate the inter-dependencies between different spatial graphs in the temporal dimension.

As indicated by the Fig. 1a, the inter-temporal graph block takes the embeddings of nodes and graph as input of the embedding fusion layer. The process can be defined as:

$$\mathbf{h}_i^{fuse}(t) = fusion\left(\mathbf{h}_i^{spa}(t), \mathbf{h}^{\mathcal{G}}(t)\right) \quad (10)$$

where $\mathbf{h}_i^{spa}(t)$ denotes the v_i 's embedding at spatial graph $\mathcal{G}_{spa}(t)$, and $\mathbf{h}^{\mathcal{G}}(t)$ is the embedding of this graph. The detailed fusion operations can be expanded as:

$$fusion\left(\mathbf{h}_i^{spa}(t), \mathbf{h}^{\mathcal{G}}(t)\right) = LN\left(\sigma\left(\mathbf{W}_{fuse} \cdot \left(\mathbf{h}_i^{spa}(t) \oplus \mathbf{h}^{\mathcal{G}}(t)\right)\right)\right) \quad (11)$$

where \oplus iteratively concatenates the graph embedding with nodes embeddings within that graph, making sure the updated node embedding contains not only local neighborhood but

also global graph-level structure information. $LN(\cdot)$ is the layer normalisation operation used to improve the training speed and mitigate the overfitting [29]. The matrix form of the generated fusion embedding of one graph is $\mathbf{H}_{fuse}(t) = [\mathbf{h}_1^{fuse}(t), \mathbf{h}_2^{fuse}(t), \dots, \mathbf{h}_N^{fuse}(t)]$.

Similar to the intra correlation layer, the inter correlation layer between nodes in two consecutive spatial graphs can be formalised as:

$$A_{tem}^{i,j}(t) = c\left(\mathbf{h}_i^{fuse}(t), \mathbf{h}_j^{fuse}(t)\right) = \frac{\exp\left(\left(\mathbf{h}_i^{fuse}(t)\right)^T \cdot \mathbf{W}_{tem} \cdot \mathbf{h}_j^{fuse}(t)\right)}{\sum_{n=1}^N \exp\left(\left(\mathbf{h}_i^{fuse}(t)\right)^T \cdot \mathbf{W}_{tem} \cdot \mathbf{h}_n^{fuse}(t)\right)} \quad (12)$$

It can be observed from Eq.12 that the inter correlation layer dynamically quantify the latent correlations using fused node embeddings in temporal dimension. $A_{tem}^{i,j}$ represents the normalised correlation value of any v_i and v_j node pairs at adjacent time steps, and \mathbf{A}_{tem} records the values of learned temporal adjacency matrix.

Inter-temporal graph block employs a recursive approach to capture inter-dependencies across different time steps, which can be formulated as:

$$\begin{aligned} \mathbf{H}_{tem}(t) = & msg(\dots) \\ & msg(\mathbf{A}(t-w+2), msg(\mathbf{A}_{tem}(t-w+1), \mathbf{H}_{fuse}(t-w))) \end{aligned} \quad (13)$$

where $\mathbf{H}_{tem}(t)$ represents the updated temporal node embeddings at time step t . The depth of recursion indicates whether a long-term temporal dependencies is needed, which is controlled by an adjustable time window w . Note that $w=0$ means the node embeddings will not be updated by inter-graph message passing, and there exists $\mathbf{H}_{tem}(t) = \mathbf{H}_{fuse}(t)$.

The final node embeddings are expected to comprise both topological spatial and inter-dependent temporal information. It can thus be derived as:

$$\hat{\mathbf{H}}_{emb}(t) = \sigma\left(\mathbf{W}_o \cdot \left(\mathbf{H}_{spa}^L(t) \oplus \mathbf{H}_{tem}(t)\right)\right) \quad (14)$$

where \mathbf{W}_o is a linear output layer. $\hat{\mathbf{H}}_{emb}(t)$ is input for the row-wise mean function $f_{mn}(\cdot)$ to generate the logits of this graph $\tilde{\mathbf{z}}(t)$, which can be used in downstream classification tasks.

$$\tilde{\mathbf{z}}(t) = softmax\left(f_{mn}\left(\hat{\mathbf{H}}_{emb}(t)\right)\right) \quad (15)$$

Specifically, we adopt binary cross-entropy loss function to train the graph classification tasks in this work.

$$\begin{aligned} \mathcal{L}_{DIIG} = & \sum_i [\tilde{z}_i(t) \cdot \log y_i(t) \\ & + (1 - \tilde{z}_i(t)) \cdot (1 - \log y_i(t))] \end{aligned} \quad (16)$$

C. Federated Relevance Module

We also design the federated relevance module, in which different participants can train a well-generalised model by considering the divergent local data distributions.

Given K participants, the local data at participant k is denoted as $\mathcal{S}^{(k)} \in \mathbb{R}^{T^{(k)} \times N \times D}$ (as explained in Section III-A), which can be reshaped to $\tilde{\mathcal{S}}^{(k)} = \left\{ \tilde{\mathbf{s}}_t^{(k)} \right\}_{t=1}^{T^{(k)}} \in \mathbb{R}^{T^{(k)} \times ND}$, and $T^{(k)}$ is the number of datapoints at participant k . As pointed out in related research [30], [31], it is intractable to compute local data distribution $p_{data}(\tilde{\mathbf{s}}^{(k)})$ due to the undifferentiable marginal likelihood. To circumvent this problem, we intend to discover a latent space where encoded representations $\mathbf{z}^{(k)}$ can be learned to characterise the local data distribution $p_{data}(\tilde{\mathbf{s}}^{(k)})$ instead. Variational autoencoder (VAE) is considered as an ideal fit for this scenario as it uses a multivariate Gaussian to model the distribution of the latent space, which is defined as $q_{\phi}(\mathbf{z}_i^{(k)} | \tilde{\mathbf{s}}_i^{(k)}) = \mathcal{N}(\mathbf{z}_i^{(k)}; \mu_i^{(k)}, \sigma_i^{2(k)} \mathbf{I})$ [30] [31]. The variational parameter ϕ in the probabilistic encoder can be learnt beforehand. The mean μ_i and s.d. σ_i are outputs of the probabilistic encoder.

We collect the latent representations $\mathbf{z}_i^{(k)}$ of each data point $\tilde{\mathbf{s}}_i^{(k)}$. The distribution representation $\mathbf{d}^{(k)}$ of $\mathcal{S}^{(k)}$ can be derived from:

$$\mathbf{d}^{(k)} = \frac{1}{T^{(k)}} \sum_{i=1}^{T^{(k)}} \mathbf{z}_i^{(k)} \quad (17)$$

We define a learnable global distribution estimator $g_{\theta}^{(k)}(\cdot)$ at each participant to approximate the global data representation, the approximate global representation from participant k is calculated as:

$$\hat{\mathbf{d}}^{(k)} = g_{\theta}^{(k)}(\mathbf{d}^{(k)}) \quad (18)$$

where θ is parameterised by an MLP. The update of θ is an integral part of the federated learning process and will be explained in the following part.

Each participant then uploads the latent local distribution vector, approximated global distribution vector and trainable weight sets $\Theta^{(k)}$ of DIIG to the server side for global model update.

$$\tilde{\mathbf{d}} = \frac{1}{K} \sum_{k=1}^K \hat{\mathbf{d}}^{(k)} \quad (19)$$

$$r^{(k)} = \frac{\exp\left(\|\hat{\mathbf{d}}^{(k)} - \tilde{\mathbf{d}}\|_2\right)}{\sum_{k=1}^K \exp\left(\|\hat{\mathbf{d}}^{(k)} - \tilde{\mathbf{d}}\|_2\right)} \quad (20)$$

$$\Theta = \sum_{k=1}^K \left(r^{(k)} \cdot \Theta^{(k)} \right) \quad (21)$$

The server receives approximated global distribution vectors from different participants and uses a vector aggregator to synthesise the true global data representation $\tilde{\mathbf{d}}$ (Eq.19). Afterwards, the relevance score of each participant can be quantified using any distance-based measure like Euclidean distance in our work. $r^{(k)}$ is the relevance score of participant k , it measures how far its local distribution representation is away from the synthesised global data distribution $\tilde{\mathbf{d}}$ at the server side (Eq.20). Therefore, a larger score indicates

this local data deviates from the global one, which needs to assign more attention to calibrate. Eq.21 refers to the attentive weight aggregation to produce the global model. The advantage of this process has two folds: 1) it reflects how relevant each participant is from the perspective of the data distributions, which follows the less relevant, less obtained weight strategy; 2) the relevance score is adjusted adaptively at different communication rounds to lead to improve the generalisation ability of the global model, in which non-IID data distributions exist in different participants.

The server then delivers the global model Θ and synthesised global data distribution representation $\tilde{\mathbf{d}}$ to each participant for a local model update. The next communication round leverages both information from the server. We propose a distribution-aware loss function, which combines the loss of the updated local model and the local loss of the approximated global distribution vectors simultaneously.

$$\mathcal{L}^{(k)} = \mathcal{L}_{DIIG}^{(k)} + MSE(\hat{\mathbf{d}}^{(k)}, \tilde{\mathbf{d}}) \quad (22)$$

The gradients w.r.t DIIG and global distribution estimator at participant k can be derived from $\mathcal{L}^{(k)}$ via $\mathbf{g}_d^{(k)} = \frac{\partial \mathcal{L}^{(k)}}{\partial \Theta^{(k)}}$ and $\mathbf{g}_e^{(k)} = \frac{\partial \mathcal{L}^{(k)}}{\partial \theta^{(k)}}$, where Θ and θ are trainable weight sets of DIIG and global estimator function $g_{\theta}(\cdot)$, respectively. Afterwards, θ and Θ can be updated at each participant:

$$\theta^{(k)} = \theta^{(k)} - \gamma \mathbf{g}_e^{(k)} \quad (23)$$

$$\Theta^{(k)} = \Theta^{(k)} - \gamma \mathbf{g}_d^{(k)} \quad (24)$$

where γ is the learning rate. The full process of federated relevance training algorithm is described in Algorithm 1.

V. EXPERIMENT

We conduct extensive experiments on real-world datasets to evaluate our proposed framework from different perspectives. We aim to answer the following research questions:

- **RQ1:** How does our proposed FedRel perform compared with the baselines (centralized implementation and FedAvg) on the basis of the same feature transformation net and correlation module?
- **RQ2:** How does the DIIG contribute to the performance improvement compared with other static connectivity methods?
- **RQ3:** Which commonly used models perform well in terms of extracting the feature information from the spatial-temporal data?
- **RQ4:** What is the best GNN option when being incorporated in the DIIG?
- **RQ5:** How does the time window w in DIIG affect the performance of the framework?

A. Experiment Setup

1) **Dataset:** In our experiments, ISRUC_S3 [14] and SHL [15] are used as the benchmark dataset. ISRUC_S3¹ collects polysomnography (PSG) recordings in 10 channels

¹https://sleeptight.isr.uc.pt/?page_id=48

Algorithm 1 Federated Relevance Training

Input: the set of participant \mathcal{K} , $\tilde{\mathcal{S}}^{(k)}$ is the reshaped spatial-temporal data at participant k , learning rate γ .

- 1: Initialise $\Theta^{(k)}$ and $\theta^{(k)}$ at each participant
- 2: Compute local data latent representation $\mathbf{d}^{(k)}$ at each participant
- 3: **for** each round $t = 1, 2, \dots, n$ **do**
- 4: **for** each $k \in \mathcal{K}$ (in parallel) **do**
- 5: $\hat{\mathbf{d}}^{(k)} = g_{\theta}^{(k)}(\mathbf{d}^{(k)})$ ▷ approximate global data vector Eq.18
- 6: Upload $\Theta^{(k)}$, $\theta^{(k)}$ and $\hat{\mathbf{d}}^{(k)}$ to the server
- 7: **end for**
- 8: $\tilde{\mathbf{d}} = \frac{1}{K} \sum_{k=1}^K \hat{\mathbf{d}}^{(k)}$ ▷ server synthesise global data representation
- 9: Compute relevance scores $\mathbf{r} = \{r^{(1)}, r^{(2)}, \dots, r^{(K)}\}$ by Eq.20
- 10: $\Theta = \sum_{k=1}^K r^{(k)} \cdot \Theta^{(k)}$ ▷ attentive aggregation
- 11: Server distributes Θ and $\tilde{\mathbf{d}}$ to each participant
- 12: **for** each $k \in \mathcal{K}$ (in parallel) **do**
- 13: Update local model $\Theta^{(k)} = \Theta$
- 14: $\mathcal{L}^{(k)} = \mathcal{L}_{DIIG}^{(k)} + MSE(\hat{\mathbf{d}}^{(k)}, \tilde{\mathbf{d}})$ ▷ compute loss for next round
- 15: Compute estimator's gradient $\mathbf{g}_e^{(k)} = \frac{\partial \mathcal{L}^{(k)}}{\partial \theta^{(k)}}$
- 16: Compute DIIG's gradient $\mathbf{g}_d^{(k)} = \frac{\partial \mathcal{L}^{(k)}}{\partial \Theta^{(k)}}$
- 17: $\theta^{(k)} = \theta^{(k)} - \gamma \mathbf{g}_e^{(k)}$
- 18: $\Theta^{(k)} = \Theta^{(k)} - \gamma \mathbf{g}_d^{(k)}$ ▷ local model update
- 19: **end for**
- 20: **end for**

TABLE II
SHARED PARAMETER SETUP IN DIIG

Name	Setup
Readout func (GNN)	2 linear layers, 1 output layer
Layer depth (GNN)	2
Loss function	Cross entropy loss
Optimiser	Adam [32]
Learning rate	1.5e-3
Dropout rate	0.3
Weight initialiser	Xavier [33]
Communication round	150

from 10 healthy subjects (i.e., sleep experiment participants). These PSG recordings are labeled with five different sleep stages according to the American academy of sleep medicine (AASM) standard [34], including Wake, N1, N2, N3 and REM. The SHL dataset contains multi-modal signal data from a body-worn camera and from 4 smartphones being equipped at various body locations. The SHL_Small² is a concise version of SHL, which contains labelled locomotion signals with different motions, including Stay Still, Walk, Run, and Train.

2) *Data Partition:* In the experiment, we randomly select 80% as the global training data and 20% as the global test set. For the training data of each participant, we emulate the partial non-IID data setup in real-world and draw the respective

²https://www.dropbox.com/s/gqlquj6rpojq64/SHL-HUAWEI_10000s.npz?dl=0

training data for each participant from this 80% data pool [35]. To verify the scalability of the proposed framework, we set the number of participants to be $\{2, 3, 5\}$, respectively. Note that the global test set is used to verify the model performance at each communication round.

3) *Parameter Settings:* The shared parameter setup across different modules of the framework can be found in Table II. Specifically, we use Adam [32] as the optimiser with the learning rate of 1.5e-3 for all trainable models in the framework. The dropout rate [36] is set to be 0.3. We apply the same readout function for all GNN models with the architecture of a shallow MLP with [32, 64, 64] neurons at each layer. Note the input node embedding size is 32 and output graph embedding size is 64. Models are collaboratively trained for 150 communication rounds and the batch size is set to be 8 in both training and test data. All trainable parameters are initialised through Xavier [33].

4) *Comparison Methods:* As our framework is composed of three key components, we thus examine on using different models in feature transformation part, spatial-temporal graph generation part, and federated learning part.

We first consider different candidates in the feature transformation net, aiming to find the best match that is capable of deriving the high-quality features from the raw spatial-temporal data, which could be used as the initial node embedding for the spatial-temporal graph generation part. We choose CNN [28] as the default feature transformation net as it has already proven effective in our preliminary work [28]. However, we reimplement other models, which are used to process the spatial-temporal related data in other works, to verify their capability of extracting features under our framework:

- MLP-Mixer [16] is a simple yet powerful model initially designed to capture spatial location features for image data, and also found useful when processing temporal signal data.
- ConvLSTM [4] reports an excellent and consistent performance in capturing spatio-temporal correlations. It replaces the fully-connected layers commonly used in the traditional LSTM with convolutional layers.
- Bi-LSTM [5] has a structure that contains two stacked unidirectional LSTMs for both forward and backward pass. It is heavily used in processing spatial-temporal features.
- Transformer [1] is one of the most prevalent models in recent years. Apart from its great success in the natural language processing (NLP) field, it also reports a promising results in uncovering highly nonlinear and dynamical spatial-temporal dependencies.

We also explore different strategies to quantify the node correlations, which serves as the adjacency matrix of the spatial-temporal graph. As explained in Section IV-B, DIIG enables a trainable correlation uncovering and embedding update simultaneously, and other three static methods are K -Nearest Neighbor (K -NN), Pearson Correlation Coefficient (PCC) and Phase Locking Value (PLV). The different node correlation functions are described as below:

- K -NN [37] generates the adjacency matrix that only

TABLE III
SUMMARY OF COMPARISON RESULTS UNDER FEDREL FOR ISRUC_S3 AND SHL_SMALL W.R.T F1 SCORE. THE BEST RESULTS ARE MARKED IN BOLD AND UNDERLINED.

			ISRUC_S3					SHL_Small				
			CNN	MLP-Mixer	ConvLSTM	Bi-LSTM	Transformer	CNN	MLP-Mixer	ConvLSTM	Bi-LSTM	Transformer
GCN	Intra Only	K-NN	0.627	0.702	0.504	0.591	0.376	0.659	0.943	0.960	0.627	0.596
		PCC	0.775	0.713	0.632	0.574	0.496	0.881	0.947	0.958	0.621	0.591
		PLV	0.723	0.701	0.579	0.579	0.487	0.881	0.958	0.947	0.631	0.604
	Inter-Intra	DIIG($w = 2$)	0.804	<u>0.794</u>	<u>0.703</u>	<u>0.679</u>	0.612	0.891	<u>0.972</u>	<u>0.967</u>	<u>0.804</u>	0.625
		DIIG($w = 3$)	<u>0.814</u>	0.792	0.681	0.655	<u>0.618</u>	<u>0.893</u>	0.967	0.957	0.788	<u>0.638</u>
		DIIG($w = 4$)	0.785	0.768	0.625	0.634	0.609	0.887	0.952	0.952	0.773	0.609
GAT	Intra Only	K-NN	0.812	0.770	0.585	0.571	0.402	0.902	0.957	0.967	0.625	0.599
		PCC	0.806	0.818	0.552	0.591	0.426	0.909	0.962	0.952	0.631	0.620
		PLV	0.816	0.817	0.563	0.628	0.420	0.911	0.962	0.964	0.651	0.623
	Inter-Intra	DIIG($w = 2$)	0.837	0.830	0.682	0.718	0.630	<u>0.931</u>	<u>0.981</u>	<u>0.974</u>	<u>0.894</u>	<u>0.635</u>
		DIIG($w = 3$)	<u>0.855</u>	<u>0.831</u>	<u>0.712</u>	<u>0.628</u>	0.928	0.973	0.966	0.888	0.886	0.614
		DIIG($w = 4$)	0.827	0.825	0.693	0.704	0.615	0.921	0.958	0.957	0.886	0.621
GPS	Intra Only	K-NN	0.764	0.679	0.579	0.541	0.426	0.866	0.950	0.958	0.880	0.596
		PCC	0.731	0.743	0.565	0.592	0.388	0.914	0.946	0.957	0.892	0.612
		PLV	0.804	0.710	0.622	0.547	0.424	0.902	0.952	0.961	0.886	0.590
	Inter-Intra	DIIG($w = 2$)	<u>0.808</u>	<u>0.748</u>	0.632	<u>0.685</u>	<u>0.602</u>	<u>0.918</u>	<u>0.957</u>	<u>0.969</u>	<u>0.902</u>	<u>0.761</u>
		DIIG($w = 3$)	0.792	0.742	0.641	0.624	0.552	0.893	0.948	0.952	0.895	0.747
		DIIG($w = 4$)	0.787	0.768	<u>0.647</u>	0.675	0.583	0.902	0.945	0.952	0.891	0.742
GraphSAGE	Intra Only	K-NN	0.714	0.721	0.545	0.570	0.433	0.887	0.958	0.961	0.628	0.642
		PCC	0.741	0.720	0.564	0.555	0.391	0.790	0.956	0.948	0.628	0.614
		PLV	0.793	0.729	0.563	0.581	0.453	0.887	0.958	0.954	0.625	0.579
	Inter-Intra	DIIG($w = 2$)	<u>0.829</u>	0.821	<u>0.727</u>	<u>0.701</u>	0.596	<u>0.922</u>	<u>0.968</u>	0.958	<u>0.683</u>	<u>0.669</u>
		DIIG($w = 3$)	0.820	0.826	0.715	0.664	<u>0.618</u>	0.901	0.957	<u>0.961</u>	0.639	0.595
		DIIG($w = 4$)	0.798	<u>0.828</u>	0.683	0.696	0.603	0.914	0.955	0.962	0.639	0.613

selects the k -th nearest neighbor of each node to represent the node correlation of the graph.

- PCC [38] is known as the Pearson correlation function to measure similarity between each pairs of nodes.
- PLV [39] is a time-dependent node correlation function to measure signals of each pairs of nodes.

Regarding the GNN used in the DIIG for each participant (shown in Fig. 1.a), we compare the following models:

- GCN [40] is the first order approximation to spectral GNN model.
- GraphSAGE [41] is the first type of GNN that introduces sampling technique, enabling a good model generalisation on unseen nodes.
- GPS [42] introduces an adaptive sampling technique, reporting good results on graph representation learning.
- GAT [27] is the first work that incorporates the attention mechanism in GNN, computing attention scores for all connected node pairs.

When it comes to the FL setup, we compare our proposed FedRel with both centralized training and FedAvg [13]. Note that only the trainable weights in DIIG unit and the global distribution estimator at participant side contribute to the federated learning process (as indicated in Fig. 1b), and the feature transformation net only serves as the pre-trained model, which shares the same parameters across different participants.

B. Experiment Results and Analysis

In this part, we evaluate the performance of our proposed framework by conducting comprehensive experiments and analysis. It essentially helps us to understand the significance of each each modules under different settings separately.

1) *Performance Analysis*: The performance of FedRel and DIIG are analysed separately.

FedRel Performance (RQ1): We first compare the overall performance of our proposed framework with both FedAvg

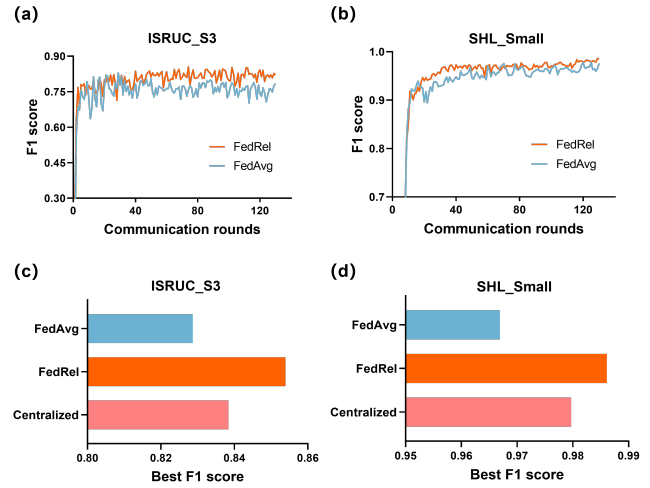


Fig. 2. Comparison of the F1 of our framework with FedAvg and Centralized settings.

and Centralized setting. Note that all other modules, including the feature transformation net and GNN model, are cherry-picked based on the best results reported in Table III (detailed analysis unveiled in ablation study). Herein, the framework is composed of CNN_GAT_DIIG_FedRel ($w = 3$) for ISRUC_S3 and MLP-Mixer_GAT_DIIG_FedRel ($w = 2$) for SHL_Small, both using GAT in DIIG module. For a fair comparison, the FedAvg and Centralized are under the same module selection.

Fig. 2 reports the performance of the proposed framework and baseline methods in terms of the best F1 score metrics, FedRel demonstrates better results compared with others on both datasets. Specifically, for the best F1 score metrics, FedRel is better than the Centralized by around 1.8% while having around 3% improvement compared with FedAvg on ISRUC_S3 (Fig. 2c).

TABLE IV

PERFORMANCE COMPARISON OF DIFFERENT PARTICIPANTS (BEST ACCURACY (ACC) AND F1 SCORE AT DIFFERENT COMMUNICATION ROUNDS).

		# of Participant		
		2	3	5
ISRUC_S3	ACC	0.8736	0.8722	0.8698
	Round	28	55	72
	F1	0.8558	0.8547	0.8431
	Round	33	52	73
SHL_Small	ACC	0.9889	0.9883	0.9886
	Round	47	72	128
	F1	0.9865	0.9859	0.9816
	Round	44	77	128

It shows a similar result on SHL_Small dataset (Fig. 2d), and FedRel still achieves the best results compared with the other two and even enjoys a larger increase compared with FedAvg (around 4%). Fig. 2a and Fig. 2b show the F1 test score curve over communication rounds. It can be observed that the FedAvg experiences a slightly stronger oscillation on both datasets, while FedRel maintains a better performance throughout the training process. There is no significant difference in terms of convergence speed on ISRUC_S3, yet it can be seen that the FedRel can converge faster and demonstrate a more stable performance than FedAvg on SHL_Small (around 40 communication rounds for FedRel and 60 for FedAvg, respectively). In general, the numerical results in Fig. 2 demonstrate that, under the same models setup, FedRel achieves a better performance compared with baselines.

We also explore the effect of the number of participants on the performance of FedRel. As shown in Table IV, we set the number of participants to be $\{2, 3, 5\}$ in our framework and record data based on two metrics, performance (represented by the best Accuracy and F1 Scores) and communication rounds. Note that the training data being assigned to each participant follows the partial non-IID data distribution. It can be clearly observed that the performance of the framework decreases slightly with the increase in the number of participants on both datasets, and the degradation is acceptable (around 1% in ISRUC_S3 and negligible in SHL_Small). We also notice that the increasing number of participants leads to more required communication rounds when achieving the best results. The rationale is that the increase of participants essentially results in a more strict non-IID data distribution, thus requiring more weight updates to converge. This part of experiments indicates the stable scalability of our proposed framework and its potential to be deployed in a real-world environment.

DIIG Performance (RQ2): It is worth mentioning that the comparison between DIIG and other static correlation functions is intractable as DIIG considers the concept of inter-intra and takes at least two temporal graph snippets as input. Static correlation functions can only draw the connectivity of nodes on each spatial graph at one time step. As depicted in Table III, the DIIG, regardless of combined feature transformation nets and GNNs, and the selections of time window w , achieves performance improvements on graph-level classification tasks

compared with most static correlation methods. Intuitively, this result verifies that the inter-dependencies in the temporal dimension contain valuable topological information from the GNN's perspective, which is critical and helpful for learning the respective embedding of nodes and graphs.

2) Comprehensive Ablation Study: We conduct comprehensive ablation studies in this part, while taking a close look at each module in our framework.

Spatial-temporal Data Processing (RQ3): As shown in Fig 1, the performance of different models adopted to generate initial node features is first studied. We implement different feature transformation models while having other modules fixed for fair comparison. To be more specifically, the results of CNN_GNN_FedRel, MLP-Mixer_GNN_FedRel, ConvLSTM_GNN_FedRel, Bi-LSTM_GNN_FedRel and Transformer_GNN_FedRel are gathered for comparison.

It can be found in Table III that the initial node features generated by CNN helps our framework achieve the best results in ISRUC_S3 dataset. Specifically, CNN improves by 12.39% on average across different GNN models. On the other hand, MLP-Mixer generates a better quality of initial node features than CNN in the SHL_Small dataset, achieving an average 9.8% improvement. It is found that for smaller spatial-temporal dataset (SHL_Small with hours of temporal sequence with only four labels), the MLP-Mixer is able to extract the critical features much more effective compared with other complex models.

GNN Models for Graph Learning (RQ4): When it comes to discovering the best match of the GNN model in DIIG, we first fix the choices of feature transformation net for each dataset and examine the results when deploying different GNN models. It can be observed that, in most cases, GAT achieves the best results compared with other GNN models. It proves that the attention-based weighted message passing in GAT also excels in the graphs containing only a small number of nodes (10 nodes per graph in ISRUC_S3 and four nodes per graph in SHL_Small).

Impact of Time Window w (RQ5): To answer RQ5, the effect of time window w in DIIG is analysed. As observed in Table III, the DIIG generally achieves the best results when $w = 2$ or $w = 3$, and it varies slightly based on the combinations of feature transformation nets and GNN models. We take a close look at the CNN_GAT and MLP-Mixer_GAT combinations, both of which achieve the best results in their respective datasets. For CNN_GAT in ISRUC_S3, DIIG reaches the best at $w = 3$, while MLP-Mixer_GAT, on the other hand, attains the most prominent result when $w = 2$. This result attributes to the length of time sequence in each dataset. In other words, ISRUC_S3 collects days of spatial-temporal signal sequences, it is thus less sensitive to the slight increase of the w (from 2 to 3). SHL_Small, on the other hand, composes only a fraction of the ISRUC_S3's sequence length and is much easier to cause the overfitting problem with the increase of w . Therefore, we use CNN_GAT_DIIG($w = 3$) and MLP-Mixer_GAT_DIIG($w = 2$) as the ideal setup of each dataset in our experiment.

VI. CONCLUSION AND FUTURE WORK

In this paper, we propose an adaptive federated relevance framework for collaborative spatial-temporal graph learning. The feature transformation net module first extracts the important spatial-temporal feature information from the raw input data, followed by a dynamic inter-intral graph (DIIG) module to generate the spatial-temporal graphs while capturing inter-dependencies and dynamic temporal changes across these graphs. Most importantly, the federated relevance module facilitates the collaborative training of DIIGs from different participants, enabling an attentive weight aggregation on the basis of diverse data distributions. The effectiveness and superiority of the proposed framework are verified through extensive experiments with a variety of variants and baseline methods. Detailed ablation studies also demonstrate the design rationale of all key components. Finally, we believe that our proposed approach provides a general framework for better exploiting the spatial-temporal data in graph forms from different participants while respecting data privacy at the same time. In future work, we will explore new strategies that could take advantage of both feature and label space when it comes to calculating the local data distribution representations.

REFERENCES

- [1] M. Xu, W. Dai, C. Liu, X. Gao, W. Lin, G.-J. Qi, and H. Xiong, “Spatial-Temporal Transformer Networks for Traffic Flow Forecasting,” *arXiv preprint arXiv:2001.02908*, 2020.
- [2] J. Zhang and Y. Wu, “A New Method for Automatic Sleep Stage Classification,” *IEEE Transactions on Biomedical Circuits and Systems*, vol. 11, pp. 1097–1110, 2017.
- [3] X. Wang, Y. Ma, Y. Wang, W. Jin, X. Wang, J. Tang, C. Jia, and J. Yu, “Traffic Flow Prediction via Spatial Temporal Graph Neural Network,” in *Proceedings of the Web Conference*, 2020, pp. 1082–1092.
- [4] X. Shi, Z. Chen, H. Wang, D. Y. Yeung, W. K. Wong, and W. c. Woo, “Convolutional LSTM Network: A machine Learning Approach for Precipitation nowcasting,” in *Advances in Neural Information Processing Systems*, 2015, pp. 802–810.
- [5] H. Zheng, F. Lin, X. Feng, and Y. Chen, “A Hybrid Deep Learning Model With Attention-Based Conv-LSTM Networks for Short-Term Traffic Flow Prediction,” *IEEE Transactions on Intelligent Transportation Systems*, vol. 22, pp. 6910–6920, 2020.
- [6] Z. Jia, Y. Lin, J. Wang, X. Ning, Y. He, R. Zhou, Y. Zhou, and L.-w. H. Lehman, “Multi-View Spatial-Temporal Graph Convolutional Networks With Domain Generalization for Sleep Stage Classification,” *IEEE Transactions on Neural Systems and Rehabilitation Engineering*, vol. 29, pp. 1977–1986, 2021.
- [7] A. Jain, A. R. Zamir, S. Savarese, and A. Saxena, “Structural-RNN: Deep Learning on Spatio-Temporal Graphs,” in *Proceedings of the IEEE Conference on Computer Vision and Pattern Recognition*, 2016, pp. 5308–5317.
- [8] B. Yu, H. Yin, and Z. Zhu, “Spatio-Temporal Graph Convolutional Networks: A Deep Learning Framework for Traffic Forecasting,” in *Proceedings of the Twenty-Seventh International Joint Conference on Artificial Intelligence*, 2018, pp. 3634–3640.
- [9] Z. Wu, S. Pan, G. Long, J. Jiang, X. Chang, and C. Zhang, “Connecting The Dots: Multivariate Time Series Forecasting with Graph Neural Networks,” in *Association for Computing Machinery’s Special Interest Group on Knowledge Discovery and Data Mining*, 2020, pp. 753–763.
- [10] Y. Seo, M. Defferrard, P. Vandergheynst, and X. Bresson, “Structured Sequence Modeling with Graph Convolutional Recurrent Networks,” in *Proceedings of the International Conference on Neural Information Processing*, 2018, pp. 362–373.
- [11] S. Yan, Y. Xiong, and D. Lin, “Spatial Temporal Graph Convolutional Networks for Skeleton-Based Action Recognition,” in *The Association for the Advance of Artificial Intelligence*, 2018, pp. 7444–7452.
- [12] P. Kairouz, H. B. McMahan, B. Avent, A. Bellet, M. Bennis, A. N. Bhagoji, K. Bonawitz, Z. Charles, G. Cormode, R. Cummings *et al.*, “Advances and Open Problems in Federated Learning,” *Foundations and Trends in Machine Learning*, pp. 1–210, 2021.
- [13] B. McMahan, E. Moore, D. Ramage, S. Hampson, and B. A. y Arcas, “Communication-Efficient Learning of Deep Networks From Decentralized Data,” in *Proceedings of the International Conference on Artificial Intelligence and Statistics*, 2017, pp. 1273–1282.
- [14] S. Khalighi, T. Sousa, J. M. Santos, and U. Nunes, “ISRUC-Sleep: A Comprehensive Public Dataset for Sleep Researchers,” *Computer Methods and Programs in Biomedicine*, vol. 124, pp. 180–192, 2016.
- [15] L. Wang, H. Gjoreski, M. Ciliberto, S. Mekki, S. Valentini, and D. Roggen, “Enabling Reproducible Research in Sensor-Based Transportation Mode Recognition With the Sussex-Huawei Dataset,” *IEEE Access*, vol. 7, pp. 10870–10891, 2019.
- [16] B. Huang, W. Chen, C.-L. Lin, C.-F. Juang, and J. Wang, “MLP-BP: A Novel Framework for Cuffless Blood Pressure Measurement with PPG and ECG Signals Based on MLP-Mixer Neural Networks,” *Biomedical Signal Processing and Control*, vol. 73, p. 103404, 2022.
- [17] D. Ienco and R. Interdonato, “Deep Multivariate Time Series Embedding Clustering via Attentive-Gated Autoencoder,” in *Pacific-Asia Conference on Knowledge Discovery and Data Mining*, 2020, pp. 318–329.
- [18] Z. Wu, S. Pan, F. Chen, G. Long, C. Zhang, and S. Y. Philip, “A Comprehensive Survey on Graph Neural Networks,” *IEEE Transactions on Neural Networks and Learning Systems*, vol. 32, pp. 4–24, 2020.
- [19] M. Defferrard, X. Bresson, and P. Vandergheynst, “Convolutional Neural Networks on Graphs with Fast Localized Spectral Filtering,” in *Proceedings of the International Conference on Neural Information Processing Systems*, 2016, pp. 3837–3845.
- [20] H. Zhang, T. Shen, F. Wu, M. Yin, H. Yang, and C. Wu, “Federated Graph Learning – A Position Paper,” *arXiv preprint arXiv:2105.11099*, 2021.
- [21] Y. Zhao, M. Li, L. Lai, N. Suda, D. Civin, and V. Chandra, “Federated Learning with Non-IID Data,” *arXiv preprint arXiv:1806.00582*, 2018.
- [22] T. Tuor, S. Wang, B. J. Ko, C. Liu, and K. K. Leung, “Overcoming Noisy and Irrelevant Data in Federated Learning,” in *International Conference on Pattern Recognition*, 2021, pp. 5020–5027.
- [23] N. Yoshida, T. Nishio, M. Morikura, K. Yamamoto, and R. Yonetani, “Hybrid-FL: Cooperative Learning Mechanism Using Non-IID Data in Wireless Networks,” in *IEEE International Conference on Communications*, 2020, pp. 1–7.
- [24] M. Shin, C. Hwang, J. Kim, J. Park, M. Bennis, and S.-L. Kim, “XOR Mixup: Privacy-Preserving Data Augmentation for One-Shot Federated Learning,” *arXiv preprint arXiv:2006.05148*, 2020.
- [25] S. Ji, S. Pan, G. Long, X. Li, J. Jiang, and Z. Huang, “Learning Private Neural Language Modeling with Attentive Aggregation,” in *International Joint Conference on Neural Networks*, 2019, pp. 1–8.
- [26] K. Xu, W. Hu, J. Leskovec, and S. Jegelka, “How Powerful Are Graph Neural Networks?” in *International Conference on Learning Representations*, 2019, pp. 1–17.
- [27] P. Veličković, G. Cucurull, A. Casanova, A. Romero, P. Lio, and Y. Bengio, “Graph Attention Networks,” in *International Conference on Learning Representations*, 2017, pp. 1–12.
- [28] G. Lou, Y. Liu, T. Zhang, and X. Zheng, “STFL: A Temporal-Spatial Federated Learning Framework for Graph Neural Networks,” *arXiv preprint arXiv:2111.06750*, 2021.
- [29] J. L. Ba, J. R. Kiros, and G. E. Hinton, “Layer normalization,” *arXiv preprint arXiv:1607.06450*, 2016.
- [30] D. P. Kingma and M. Welling, “Auto-encoding variational bayes,” in *International Conference on Learning Representations*, 2014, pp. 1–14.
- [31] S. Zhao, J. Song, and S. Ermon, “Towards deeper understanding of variational autoencoding models,” in *International Conference on Machine Learning*, 2017, pp. 1–9.
- [32] D. P. Kingma and J. Ba, “Adam: A Method for Stochastic Optimization,” in *International Conference on Learning Representations*, 2015, pp. 1269–1272.
- [33] X. Glorot and Y. Bengio, “Understanding the Difficulty of Training Deep Feedforward Neural Networks,” in *International Conference on Artificial Intelligence and Statistics*, 2010, pp. 249–256.
- [34] Z. Jia, Y. Lin, J. Wang, R. Zhou, X. Ning, Y. He, and Y. Zhao, “Graph-SleepNet: Adaptive Spatial-Temporal Graph Convolutional Networks for Sleep Stage Classification,” in *Proceedings of the International Joint Conference on Artificial Intelligence*, 2020, pp. 1324–1330.
- [35] T. Zhang, Z. Shen, J. Jin, X. Zheng, A. Tagami, and X. Cao, “Achieving Democracy in Edge Intelligence: A Fog-Based Collaborative Learning Scheme,” *IEEE Internet of Things Journal*, vol. 8, pp. 2751–2761, 2020.
- [36] N. Srivastava, G. Hinton, A. Krizhevsky, I. Sutskever, and R. Salakhutdinov, “Dropout: A Simple Way to Prevent Neural Networks from Overfitting,” *The Journal of Machine Learning Research*, vol. 15, pp. 1929–1958, 2014.

- [37] B. Jiang, C. Ding, B. Luo, and J. Tang, "Graph-Laplacian PCA: Closed-Form Solution and Robustness," in *Proceedings of the IEEE Conference on Computer Vision and Pattern Recognition*, 2013, pp. 3492–3498.
- [38] K. Pearson and A. Lee, "On the Laws of Inheritance In Man: I. Inheritance of Physical Characters," *Biometrika*, vol. 2, pp. 357–462, 1903.
- [39] S. Aydore, D. Pantazis, and R. M. Leahy, "A Note on The Phase Locking Value and its Properties," *Neuroimage*, vol. 74, pp. 231–244, 2013.
- [40] T. N. Kipf and M. Welling, "Semi-Supervised Classification with Graph Convolutional Networks," in *International Conference on Learning Representations*, 2017, pp. 1–14.
- [41] W. Hamilton, Z. Ying, and J. Leskovec, "Inductive Representation Learning on Large Graphs," in *Advances in Neural Information Processing Systems*, 2017, pp. 1024–1034.
- [42] T. Zhang, Y. Liu, X. Chen, X. Huang, F. Zhu, and X. Zheng, "GPS: A Policy-driven Sampling Approach for Graph Representation Learning," *arXiv preprint arXiv:2112.14482*, 2021.